ACS OMEGA

http://pubs.acs.org/journal/acsodf

Article

Stereoselective Synthesis of Spirooxindole Derivatives Using One-Pot Multicomponent Cycloaddition Reaction and Evaluation of Their Antiproliferative Efficacy

Rajat Ghosh, Jorge B. Vitor, Eduarda Mendes, Alexandra Paulo, and Pratap Chandra Acharya*

Cite This: *ACS Omega* 2020, 5, 27332−27343

Read Online

ACCESS | Metrics & More | Article Recommendations | Supporting Information

ABSTRACT: A highly stereoselective, one-pot, multicomponent method has been developed to synthesize pyrrolizidine- and *N*-methyl pyrrolidine-substituted spirooxindole derivatives. The [3 + 2] cycloaddition reaction involves the reaction between the dipole azomethine ylides, generated *in situ* from the reaction between isatin and secondary amino acids such as L-proline or sarcosine, and *α,β*-unsaturated carbonyl compounds as the dipolarophile. The reaction condition was optimized to achieve excellent regio- and stereoselectivity. Products were obtained in good yield using ethanol as a solvent at the reflux temperature. The newly synthesized spirooxindole derivatives were evaluated for their antiproliferative efficacy against National Cancer Institute (NCI)-60 cancer cell lines and DNA G-quadruplex (G4) interaction capacity. Compound **14b** produced selective cytotoxicity against leukemia, renal, colon, and prostate cancer cell lines at a 10 *μ*M concentration. The G4 interaction studies further suggested that these spirooxindole derivatives were devoid of any activity as DNA G4 ligands.

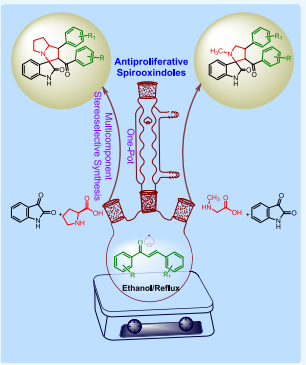

1. INTRODUCTION

The search for a cancer chemotherapeutic agent with better efficacy and less toxicity endures a challenge for a new drug discovery process and has always compelled medicinal chemists to discover innovative agents with cancer selectivity.[1] Isatin-inspired spirooxindole derivatives are a highly precious synthetic framework due to their diversified biological properties including the antiproliferative activity.[2,3] Spirooxindoles are found in several bioactive natural products such as coerulescine, horsfiline, spirotryprostatin A, welwitindolinone A, elacomine, and alstonisine.[3] The synthetic spirooxindoles have also been found to possess various biological properties such as progesterone receptors modulators, anti-human immunodeficiency virus (HIV), anticancer, antitubercular, antimalarial, and mouse double minute 2 (MDM2) inhibitor.[4−6]

The halogenated spirooxindole derivatives NITD609 (**1**) and MI-888 (**2**) (Figure 1) exhibited efficiency in nanomolar concentration for the treatment of malaria and cancer, respectively.[4] The methoxyphenyl spirooxindole **3** and the halogenated derivative **4** also displayed potent activity against bacterial cell division and *Mycobacterium tuberculosis* H37Rv, respectively (Figure 1).[7] In the recent past, several spirooxindole derivatives have been studied against U937 human histiocytic lymphoma, B16F10 mouse melanoma, U87 human glioma, and MDM2-p53 protein−protein interaction and found to possess moderate to good anticancer efficacy.[8−12]

Various synthetic protocols have been reported for the preparation of biologically active spirooxindole scaffolds, and isatin-inspired multicomponent [3 + 2] cycloaddition reaction

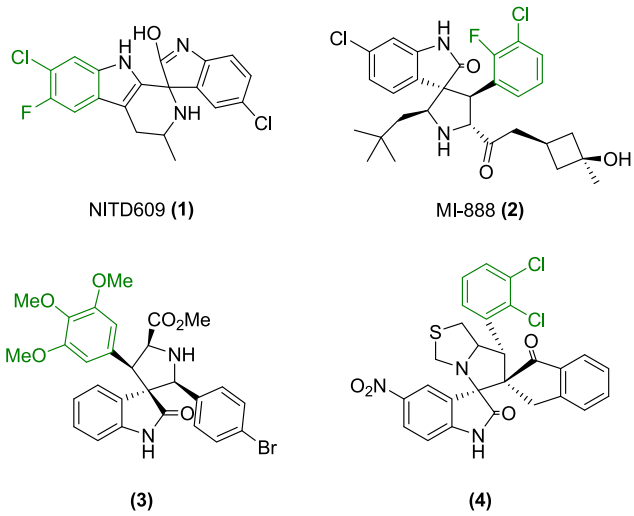

Figure 1. Biologically active spirooxindole derivatives.

is one of them.[4,5] The spiro annulation reactions on the C-3 carbonyl function of isatin can be utilized to build several types

Received: July 31, 2020
Accepted: October 5, 2020
Published: October 16, 2020

https://dx.doi.org/10.1021/acsomega.0c03675
ACS Omega 2020, 5, 27332−27343

of spiro-fused heterocyclic and carbocyclic frameworks, including the spirooxindole derivatives.[6,7] The cycloaddition of the dipole azomethine ylide, which is produced *in situ* by the reaction between isatin and secondary amino acids, to a dipolarophile results in a one-pot, multicomponent, [3 + 2] cycloaddition reaction, leading to stereoselective spirooxindole derivatives.[8,9] Other advantages include high regio and stereoselectivity, catalyst-free reaction, high atom economy, wide structural diversity, and suitable bond-forming efficiency in a single-step method through the formation of *in situ* azomethine ylide.[7]

The antiproliferative activity of compounds bearing pyrrolizidine and *N*-methyl pyrrolidine fragments has been evidenced by the alkaloid casuarine (**5**) and thesinine (**6**) as well as coerulescine (**7**) and horsfiline (**8**), respectively (Figure 2).[7,13] On the other hand, chalcones or *α,β*-unsaturated carbonyl compounds are also reported to have myriads of biological properties including antiproliferative activity.[14]

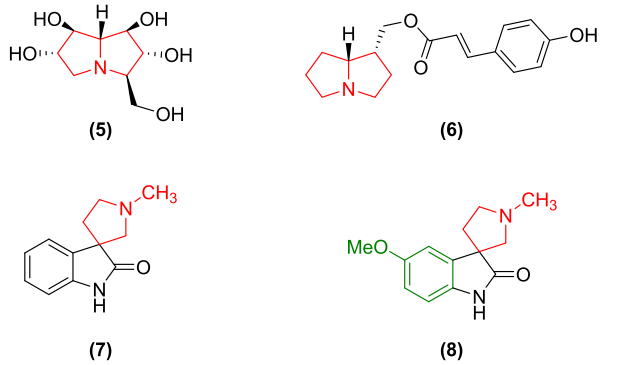

Figure 2. Bioactive molecules with pyrrolizidine (**5**,**6**) and *N*-methyl pyrrolidine (**7**,**8**) scaffolds.

In the present study, we explored the feasibility of a one-pot multicomponent cycloaddition reaction using isatin-inspired azomethine ylide as the dipole and various halogenated as well as methoxy-substituted chalcones as dipolarophiles to yield stereoselective spirooxindole derivatives. The antiproliferative efficacy of the newly synthesized spirooxindoles was evaluated against various cancer cell lines National Cancer Institute (NCI)-60 using sulforhodamine B (SRB) cytotoxicity assay.

Furthermore, it was shown that small molecules with aromatic N-heterocycles, such as the indole nucleus, were able to bind and stabilize DNA G-quadruplex (G4) structures.[15] G4 nucleic acids are known anticancer drug targets due to their involvement in several cell proliferation regulatory processes.[16] In this regard, the spirooxindole derivatives were evaluated for their capacity to induce DNA G4 and, consequently, to stop the DNA replication by a polymerase, and also to selectively stabilize G4 structures of different topologies compared to a hairpin double-stranded DNA (ds-DNA) sequence.

2. RESULTS AND DISCUSSION

2.1. Chemistry. The synthesis of the target spirooxindole derivatives was achieved using a one-pot, multicomponent, [3 + 2] cycloaddition reaction employing *α,β*-unsaturated carbonyl compounds (chalcones) as the dipolarophiles and azomethine ylides as dipoles under appropriate reaction conditions.

The Claisen−Schmidt condensation of various halogen or methoxy-substituted benzaldehydes **9** and acetophenones **10** at room temperature in alkaline medium afforded the desired *trans*-chalcones **11a−e** in good yield and were purified by recrystallization from ethanol (Scheme 1).[1,17] The carbonyl stretching vibrations of the chalcones were found at a lowered wavenumber of ∼1650 cm^{-1} due to the introduction of *α,β*-unsaturation. The proton NMR showed the distinguishing doublets of vinylic and benzylic protons at ∼*δ* 6.93 to 8.24 ppm. The *p*-methoxy-substituted derivatives **11c** showed sharp singlets at 3.85 and 3.89, whereas the singlets for 3,4,5-trimethoxy-substituted derivative **11d** appeared at 4.25 and 4.27 ppm for the protons of $-OCH_3$ in the ^1H NMR spectra. The configuration of the chalcones was confirmed to be trans (*E*) from the higher coupling constant value (*J* = 15 Hz) for both vinylic and benzylic protons, consistent with earlier reports.[7,18]

Using these *trans*-chalcones as the dipolarophiles, we investigated the reaction conditions for the synthesis of pyrrolizidine spirooxindoles through the 1,3-dipolar cyclo-

Scheme 1. Reaction and Reagents for the Synthesis of the Substituted Chalcones 11a−e: (a) NaOH, MeOH, Stirring, Room Temperature

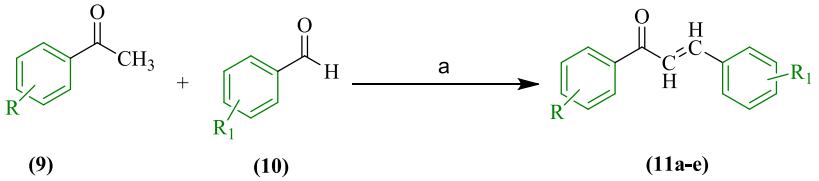

(9) (10) (11a-e)

Comp No.	R	R_1
11a	4-Br	4-Br
11b	4-Br	4-Cl
11c	4-OCH_3	4-OCH_3
11d	4-Br	5,4,3-$(OCH_3)_3$
11e	4-Br	−H

https://dx.doi.org/10.1021/acsomega.0c03675
ACS Omega 2020, 5, 27332−27343

Table 1. Optimization of Reaction Conditions

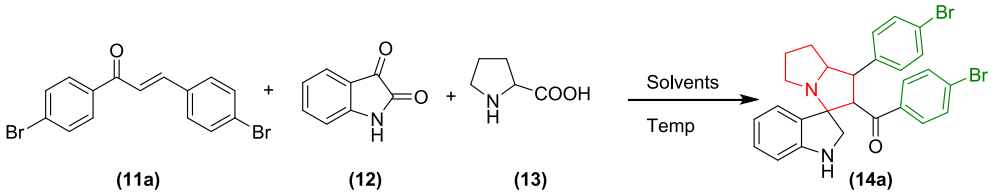

(11a) (12) (13) (14a)

entry	solvent	temperature (°C)	time (h)	yield (%)
1	toluene	rt	72	ND
2		reflux	72	ND
3	xylene	rt	72	ND
4		reflux	72	ND
5	dimethyl sulfoxide	rt	72	ND
6		reflux	72	ND
7	tetrahydrofuran	rt	72	ND
8		reflux	72	ND
9	1,4-dioxane	rt	72	ND
10		reflux	72	ND
11	acetone	rt	72	ND
12		reflux	72	ND
13	ethylmethyl ketone	rt	72	ND
14		reflux	72	ND
15	ethylacetate	rt	72	ND
16		reflux	72	ND
17	acetonitrile	rt	72	ND
18		reflux	72	ND
19	chloroform	rt	72	ND
20		reflux	72	ND
21	distilled water	rt	72	ND
22		reflux	72	ND
23	methanol	rt	72	ND
24		60 °C	72	30
25		reflux	72	47.5
26	isopropanol	rt	72	ND
27		60 °C	72	28
28		reflux	72	35
29	*n*-butanol	rt	72	ND
30		reflux	72	ND
31	ethanol	rt	72	ND
32		60 °C	24	54
33		reflux	5	89.5

The reaction was carried out with **11a**, **12**, and **13** in the ratio of 1:1.3:1.3 stirred in 10 mL of solvent. Isolated yield was calculated based on chalcone. Reaction completion was monitored by TLC. ND = not detected, rt = room temperature.

addition reaction using *in situ* generated azomethine ylide to incorporate three new bonds, four stereocenters, and one spirocyclic quaternary carbon. For this purpose, equimolar quantities of isatin (**12**), L-proline (**13**), and chalcone **11a** were taken together and stirred under various reaction conditions for the synthesis of *p*-bromophenyl-substituted pyrrolizidine spirooxindole **14a**, as shown in Table 1. Unlike the reported methods, the nonpolar solvents were unsuitable for this reaction due to lack of solubility of the starting materials, especially the secondary amino acid L-proline.[2] Polar aprotic solvents such as tetrahydrofuran (THF), dimethyl sulfoxide (DMSO), dioxane, acetone, ethylmethyl ketone, ethylacetate, and acetonitrile also did not produce desired results as the starting materials were sparingly soluble in these solvents even at the reflux temperature and longer reaction time. We further investigated the effect of various polar protic solvents like water, methanol, ethanol, isopropanol, and *n*-butanol on the solubility of the starting material and progress of the reaction. The reaction did not proceed well with water or higher alcohols due to solubility issues of chalcones. The reaction proceeded with only methanol, isopropanol, and ethanol. However, complete consumption of the chalcone was not achieved even after 72 h of reflux with equimolar quantities of isatin and L-proline, as evidenced from thin-layer chromatography (TLC). On increasing the molar ratio of isatin and L-proline to 1.3 times, the reaction proceeded toward completion only with ethanol within 5 h of reflux with good yield. Therefore, the reaction condition was optimized to use an ethanolic solution of chalcone, isatin, and L-proline in the ratio of 1:1.3:1.3 at the reflux temperature for the synthesis of spirooxindole derivatives. Subsequently, all of the pyrrolizidine spirooxindoles **14a**–**e** were synthesized from various substituted α,β-unsaturated carbonyl compounds **11a**–**e** using ethanol as a solvent (Scheme 2).

https://dx.doi.org/10.1021/acsomega.0c03675
ACS Omega 2020, 5, 27332−27343

Scheme 2. Reaction and Reagents for the Synthesis of the Pyrrolizidine Spirooxindoles 14a−e: (a) Ethanol, Reflux with Stirring, 5 h

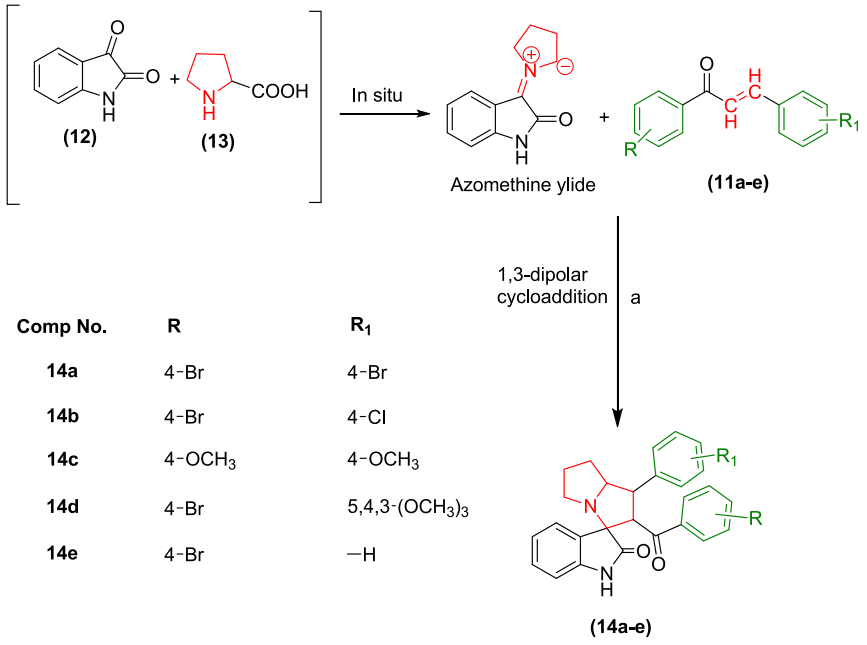

Comp No.	R	R_1
14a	4-Br	4-Br
14b	4-Br	4-Cl
14c	4-OCH_3	4-OCH_3
14d	4-Br	5,4,3-$(OCH_3)_3$
14e	4-Br	−H

The stereoselectivity of the reaction was investigated with the help of NMR spectra of the *p*-bromophenyl-substituted pyrrolizidine spirooxindole **14a** as a prototype by assigning the configuration at the stereocenters. The TLC analysis of the recrystallized product showed only a single isomer. However, there is a possibility of formation of four pairs of isomers due to the presence of four stereocenters, which cannot be detected in TLC owing to the same Rf value of stereoisomers. The proton NMR spectrum of the spirooxindole **14a** did not show any isomeric peak splitting. Further analysis of the proton NMR also confirmed that the compound is a single stereoisomer.

First, the stereochemistry of the hydrogen of amino acid L-proline is predetermined. Therefore, the configuration of the *Hd* will always be retained, and it remained below the plane at C_1 stereocenter. Second, there is a possibility of formation of either **14a(i)** or **14a(ii)** configuration with *p*-bromobenzoyl and *p*-bromophenyl groups interchanging their position at the stereocenter C_2 and C_3 (Figure 3). However, the proton NMR data and coupling constant (J) value support the formation of only **14a(i)** having the *p*-bromobenzoyl substituent at C_3 and *p*-bromophenyl substituent at C_2 stereocenters, respectively. The doublets of *Hf* appeared downfield at δ 4.81 due to the presence of adjacent −C═O function compared to the triplets of *He*, which resonated at δ 3.87 ppm. Furthermore, the appearance of doublets of *Hf* confirms that only one proton (*He*) is present in the neighborhood. The less deshielded *He* produces a triplet due to the presence of neighboring *Hf* and *Hd*. Furthermore, the multiplet of *Hd* resonates at a downfield of δ 4.22 ppm. Therefore, it is confirmed that the pyrrolizidine spirooxindoles have **14a(i)** configuration. The higher coupling constants of *He* (J = 12.00 Hz) and *Hf* (J = 11.60 Hz) support the fact that the trans orientation of *p*-bromobenzoyl and *p*-bromophenyl groups from the chalcones is retained in the product. The higher J value of *He* also implicates that it is trans to the *Hd* as well. Hence, considering below the plane orientation of *Hd*, the configuration of all of the three

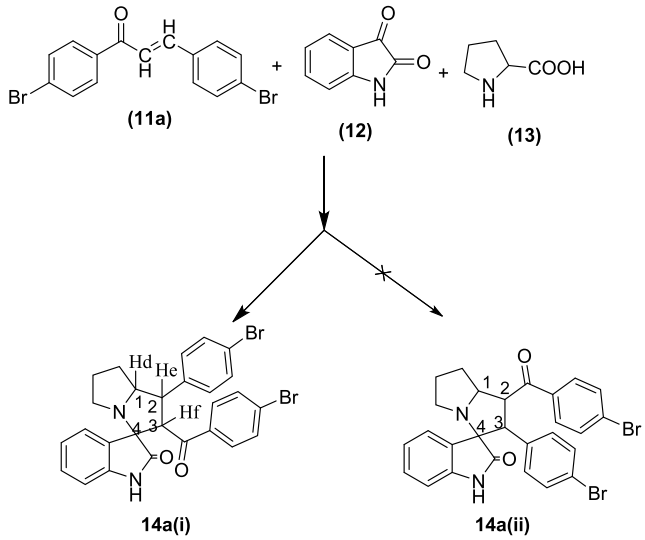

Figure 3. Pyrrolizidine spirooxindole **14a** with two tentative configurations **14a(i)** and **14a(ii)**.

hydrogens at C_1, C_2, and C_3 stereocenters can be assigned as all trans to each other to arrive at the structure of **14a**, as shown in Figure 4.

Furthermore, the stereochemistry of C_4 spiro quaternary stereocenter can also produce a pair of isomers, as shown in Figure 5. However, it is well established that the cycloaddition of azomethine ylide proceeds preferably *via* an S-shaped ylide than a W-shaped ylide due to higher stability and resonance energy of the S-shaped ylide.[7] Therefore, the orientation of C_4 stereocenter is always predetermined, thus confirming the stereochemistry of the pyrrolizidine spirooxindoles **14a**. Overall, the reaction is confirmed to be highly stereo- and regioselective, leading to the formation of only one stereoisomer.

All of the pyrrolizidine spirooxindole derivatives **14a−e** displayed similar Fourier transform infrared (FTIR), ^{1}H, and

https://dx.doi.org/10.1021/acsomega.0c03675
ACS Omega 2020, 5, 27332−27343

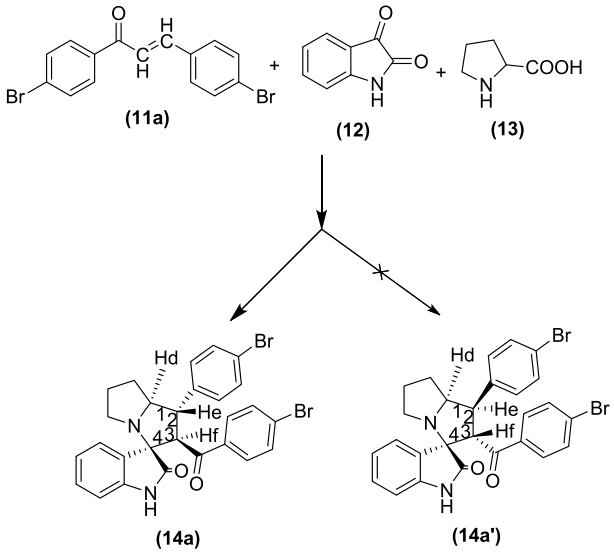

Figure 4. Pyrrolizidine spirooxindole **14a** with configurations at C1, C2, and C3 stereocenters.

^{13}C NMR spectra, confirming the formation of all of the products in agreement with the assigned stereochemistry. Aliphatic protons resonated between δ 1.50 and 4.86, and aromatic protons between δ 6.57−7.54 ppm in the ^{1}H NMR spectra. The singlet for isatin −NH was observed at $\delta \sim 7.5$ ppm. Similarly, ^{13}C NMR showed peaks for aliphatic carbon between δ 27.17 and 73.91 and aromatic carbon between 104.99 and 163.30 ppm. The two carbonyl carbons of pyrrolizidine spirooxindoles were observed between δ 180.34 and 196.13 ppm. Structures of the pyrrolizidine spirooxindole derivatives **14a−e** were further confirmed from the electrospray ionization-mass spectra (ESI-MS) and their molecular ion $[M + H]^+$ peaks. In addition to the $[M + H]^+$ peaks, the characteristic $[MH + 2]^+$ and $[MH + 4]^+$ peaks were also observed for spirooxindole derivatives **14a** due to the presence of two bromine atoms with a peak intensity ratio of 1:2:1 at m/z 565, 567, and 569, respectively. Similarly, compound **14b** carrying one bromine and one chlorine atom also displayed $[M + H]^+$, $[MH + 2]^+$, and $[MH + 4]^+$ peaks in a 3:4:1 intensity ratio at m/z 521, 523, and 525, respectively. The $[MH + 2]^+$ peak was also observed in **14d** and **14e** due to the presence of one bromine atom in each compound along with the molecular ion peak at m/z 579 and 489 in the peak intensity ratio of 1:1, respectively.

On a similar note, a series of *N*-methyl pyrrolidine-substituted spirooxindole derivatives **16a−e** were prepared employing α,β-unsaturated carbonyl compounds **11a−e**, isatin (**12**), and sarcosine (**15**) under analogous reaction conditions (Scheme 3). The reaction proceeded in accordance with the earlier experiment producing a single stereoisomer. The regioselectivity of the reaction toward the *trans*-chalcones was also retained, as evidenced by the ^{1}H NMR spectra.

The stereochemistry of the *N*-methyl pyrrolidine spirooxindole derivatives **16a−e** was confirmed based on the structural information of the earlier series of pyrrolizidine spirooxindoles derivative; ^{1}H NMR, ^{13}C NMR, and COSY spectra; and literature support.[19] The stereochemistry and orientation of protons and other substituents are portrayed in Figure 6 through the representative *N*-methyl pyrrolidine spirooxindole derivative **16a**. The carbon resonating at δ 73.47 ppm was found to be the spiro carbon as it did not show any correlation with a proton in the ^{1}H−^{13}C COSY NMR spectrum.

The infrared (IR) spectra of *N*-methyl spirooxindole derivatives **16a−e** exhibited characteristic −NH and carbonyl stretching vibrations at wavenumbers ∼3796 and ∼1690 cm^{-1}, respectively. Proton NMR showed peaks for $-N-CH_3$ at $\delta \sim$ 2.22, aliphatic protons between 3.43 and 4.57 ppm, aromatic protons between 6.51 and 7.55, and singlet of −NH between 7.61 and 8.25 ppm. Similarly, peaks for aliphatic carbons were

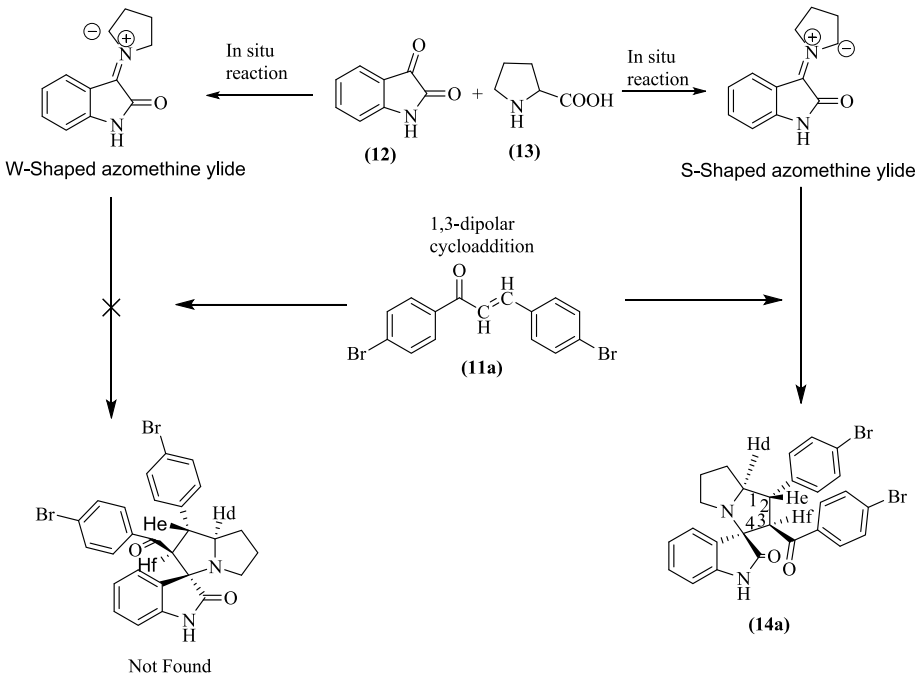

Figure 5. Formation of S-shaped and W-shaped azomethine ylides and their interaction with dipolarophile **11a**.

https://dx.doi.org/10.1021/acsomega.0c03675
ACS Omega 2020, 5, 27332−27343

Scheme 3. Reaction and Reagents for the Synthesis of the *N*-Methyl Pyrrolidine Spirooxindoles 16a−e: (a) Ethanol, Reflux with Stirring, 5 h

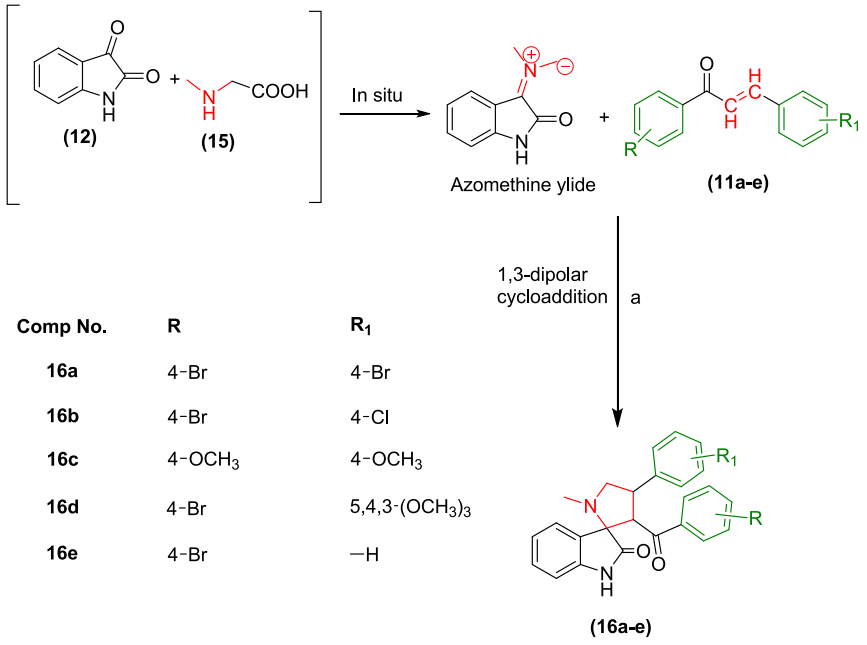

Comp No.	R	R_1
16a	4-Br	4-Br
16b	4-Br	4-Cl
16c	4-OCH_3	4-OCH_3
16d	4-Br	5,4,3-$(OCH_3)_3$
16e	4-Br	−H

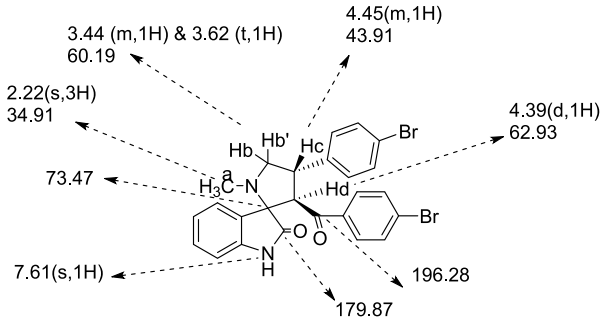

Figure 6. Assignment of ^{1}H and ^{13}C NMR chemical shifts of *N*-methyl pyrrolidine spirooxindole **16a**.

observed at δ between 34.90 and 73.58, aromatic carbons between 105.13 and 163.12, and two carbonyl carbons between 179.64 and 196.62 ppm in the ^{13}C NMR. The structures of the spirooxindole derivatives **16a−e** were further confirmed from their ESI-MS. In mass spectrum, a characteristic $[M + H]^+$ peak was observed for **16c** at m/z 443, whereas compound **16a** displayed an $[MH + 2]^+$ peak at m/z 541 and $[M - 2H]^-$, $[(M - 2H) + 2]^-$, and $[(M - 2H) + 4]^-$ peaks at m/z 536, 538, and 540, respectively, due to the presence of two bromine atoms with a peak intensity ratio of 1:2:1. Similarly, the *N*-methyl spirooxindole derivatives **16b** showed $[M - 2H]^-$, $[(M - 2H) + 2]^-$, and $[(M - 2H) + 4]^-$ peaks because of one bromine and one chlorine atom with a peak intensity ratio of 3:4:1 at m/z 492, 494, and 496, respectively. The $[(M - H) + 2]^-$ peak was also observed in **16d** and **16e** along with molecular ion peak due to the presence of one bromine atom with a peak intensity ratio of 1:1 at m/z 551 and 461, respectively.

2.2. *In Vitro* Antineoplastic Activity. *2.2.1. In Vitro Cancer Cell Line Assay.* All of the newly synthesized spirooxindole derivatives **14a−e** and **16a−e** were submitted to National Cancer Institute (NCI), Bethesda through their Developmental Therapeutics Program (DTP) for *in vitro* cytotoxicity assay on 60 different cancer cell lines of nine tissue origins.[20] The initial assay at a single dose of 10 μM concentration revealed that these compounds have selective antiproliferative properties and do not exhibit general cytotoxicity. The results of the single dose *in vitro* cytotoxicity assay are summarized in Tables 2 and 3.

The bis-*p*-bromophenyl-substituted pyrrolizidine spirooxindole derivative **14a** produced the highest growth inhibitions of 59.56% and 61.83% selectively against K-562 leukemia and UO-31 renal cancer cell line at 10 μM concentration, respectively. Furthermore, compound **14a** produced more than 50% growth inhibition against non-small cell lung cancer cell A549/ATCC, renal cancer CAKI-1, prostate cancer PC-3, breast cancer T-47D, colon cancer HCT-116, and HT29 cell lines. The *p*-bromophenyl- and *p*-chlorophenyl-substituted derivative **14b** produced approximately 50% growth inhibition against leukemia cell line MOLT-4, non-small cell lung cancer cell line A549/ATCC, colon cancer cell lines HCT-116 and HT29, CNS cancer cell line SNB-75, ovarian cancer cell line IGROV1, breast cancer cell line T-47D, and renal cancer cell lines CAKI-1 and SN12C at 10 μM concentration. Furthermore, compound **14b** showed the highest growth inhibitions of 66.46, 65.48, and 67.34% against K-562 (leukemia), UO-31 (renal cancer), and PC-3 (prostate cancer) cell lines, respectively. The *p*-bromophenyl-substituted pyrrolizidine spirooxindole **14e** also displayed approximately 50% growth inhibition against leukemia cell line K-562, non-small cell lung cancer cell line A549/ATCC, colon cancer cell line HT29, CNS cancer SNB-75, ovarian cancer cell line IGROV1, renal cancer cell line CAKI-1, and breast cancer cell lines MCF7 and T-47D. Compound **14e** showed the highest growth inhibitions of 59.57 and 65.34% against the renal cancer cell line UO-31 and prostate cancer cell line PC-3, respectively, at 10 μM concentration.

Similarly, the bis-*p*-bromophenyl-substituted *N*-methyl pyrrolidine spirooxindole derivative **16a** displayed more than 50% growth inhibition against K-562 leukemia, PC-3 prostate,

https://dx.doi.org/10.1021/acsomega.0c03675
ACS Omega 2020, 5, 27332−27343

Table 2. Percentage Growth of Cancer Cells Treated with Compounds 14a−e at a Dose of 10 μM

cell lines	compound code				
	14a	14b	14c	14d	14e
Leukemia					
CCRF-CEM	71.50	68.19	100.36	95.61	71.38
HL-60 (TB)	85.63	74.17	98.35	99.62	86.62
K-562	40.44	33.54	88.12	98.34	49.72
MOLT-4	53.06	37.57	90.22	83.28	56.82
RPMI-8226	62.07	55.63	91.70	83.11	55.71
SR	54.98	46.71	94.33	110.60	63.03
Non-Small Cell Lung Cancer					
A549/ATCC	49.62	41.79	90.47	80.73	50.05
EKVX	62.12	55.67	94.73	86.66	62.59
HOP-62	74.00	69.46	93.10	96.48	80.65
HOP-92	74.00	63.35	80.32	77.50	69.19
NCI-H226	78.73	70.15	91.57	85.55	75.18
NCI-H23	73.57	68.08	89.45	92.28	80.01
NCI-H322M	94.03	88.49	104.84	87.93	94.89
NCI-H460	66.60	55.15	101.26	96.83	61.12
NCI-H522	64.00	58.49	85.49	74.65	60.43
Colon Cancer					
COLO 205	62.68	62.49	102.44	96.67	76.94
HCC-2998	91.33	84.28	100.45	102.09	94.37
HCT-116	43.56	40.67	97.26	94.53	56.08
HCT-15	61.26	55.74	96.94	89.11	63.64
HT29	48.08	40.15	98.50	85.26	51.02
KM12	66.51	51.38	93.75	87.36	60.63
SW-620	71.04	65.24	96.16	99.75	73.74
CNS Cancer					
SF-268	65.13	60.60	92.02	75.05	65.07
SF-295	67.97	61.48	90.14	89.53	59.94
SF-539	85.06	92.12	98.89	91.03	81.48
SNB-19	69.72	67.47	86.60	81.32	70.80
SNB-75	52.87	49.29	66.80	75.35	50.69
U251	71.61	62.43	96.50	85.96	68.25
Melanoma					
LOX IMVI	81.68	69.19	87.65	87.59	75.58
MALME-3M	84.71	78.68	96.67	93.54	82.24
M14	73.67	70.35	87.71	105.17	68.36

cell lines	compound code				
	14a	14b	14c	14d	14e
Melanoma					
MDA-MB-435	77.39	67.56	96.35	96.33	70.59
SK-MEL-2	87.53	90.99	99.01	88.49	85.77
SK-MEL-28	99.31	99.47	113.51	100.52	102.38
SK-MEL-5	91.31	85.03	98.70	93.57	80.91
UACC-257	86.29	79.50	99.11	87.35	84.56
UACC-62	57.28	53.14	74.33	81.49	54.50
Ovarian Cancer					
IGROV1	58.20	47.30	83.72	93.05	49.15
OVCAR-3	80.46	66.91	102.30	92.51	72.45
OVCAR-4	72.50	64.86	83.50	90.29	65.48
OVCAR-5	79.86	78.10	99.24	90.00	85.94
OVCAR-8	70.10	63.16	93.55	90.19	68.88
NCI/ADR-RES	58.12	55.63	87.31	90.90	61.98
SK-OV-3	71.45	73.10	96.74	85.97	78.65
Renal Cancer					
786−0	77.49	75.83	101.89	101.14	83.95
A498	95.62	64.76	107.42	77.00	80.27
ACHN	73.63	69.39	92.15	98.11	70.09
CAKI-1	45.04	40.58	68.86	75.97	46.05
RXF 393	63.02	51.07	87.44	81.82	65.70
SN12C	66.79	40.76	92.66	85.18	71.35
TK-10	95.84	90.62	104.27	81.46	97.60
UO-31	38.17	34.52	56.48	79.07	40.43
Prostate Cancer					
PC-3	41.79	32.66	73.03	-	34.66
DU-145	86.15	81.52	102.88	95.82	77.79
Breast Cancer					
MCF7	56.72	46.42	101.02	93.03	52.46
MDA-MB-231/ ATCC	86.25	76.78	93.62	84.15	76.02
HS 578T	83.25	79.67	89.96	83.98	78.74
BT-549	102.10	91.99	103.03	95.83	95.00
T-47D	48.47	45.84	90.26	70.47	46.98
MDA-MB-468	84.16	82.10	111.00	79.61	72.04
mean % growth	**70.59**	**63.79**	**93.11**	**89.01**	**69.44**

T-47D breast cancer, CAKI-1, and UO-31 renal cancer cell lines at a dose of 10 μM. The highest growth inhibitions of 60.33 and 63.98% were observed against the colon cancer cell lines HCT-116 and HT29, respectively. The *p*-bromophenyl- and *p*-chlorophenyl-substituted *N*-methyl pyrrolidine spirooxindoles derivative **16b** displayed more than 50% growth inhibition only against HT29 colon cancer cell line at 10 μM concentration. All other *N*-methyl pyrrolidine spirooxindoles **16c−e** were found to be inactive against the NCI-60 cell lines.

In general, the halogenated spirooxindoles are found to produce selective cytotoxicity, whereas the methoxy-substituted derivatives are inactive. The physicochemical properties of the most active derivative **14b** have been generated using SwissADME tool and are given in Supporting Information Figure S54. The physicochemical data predict that the spirooxindole derivative is lipophilic in nature and thereby have more affinity to inhibit the central nervous system (CNS) or lung cancer, as evident from the experimental data. Further, the pyrrolizidine spirooxindole derivative **14b** emerged as a potential hit molecule and warrants further hit-to-lead optimization studies to discover a cancer chemotherapeutic drug candidate.

2.2.2. G-Quadruplex (G4) Interaction Studies. The spirooxindole derivatives **14a−e** and **16a−e** were further evaluated for their capacity to interact and stabilize DNA quadruplex structures to verify whether the selective cytotoxicity may be produced through the interaction of compounds with these regulatory nucleic acid structures. To assess this capacity, we used two complementary methodologies, following procedures previously reported by the authors.[21,22]

2.2.2.1. Polymerase-Stop Assay. The capacity of the spirooxindole derivatives **14a−e** and **16a−e** to selectively disrupt G4-DNA−polymerase interactions was evaluated using a polymerase chain reaction (PCR)-stop assay methodology and the G4-forming sequence (Pu27) controlling the transcription of c-MYC oncogene. A concentration of 100 μM was used for initial screen. The gel electrophoresis of the PCR-stop assay products presented in Figure 7 indicates that the spirooxindole derivatives **14a−e** and **16a−e** are not able to induce the formation of the G4, under the assay conditions, and subsequently stop polymerase activity.

2.2.2.2. Fluorescence Resonance Energy Transfer (FRET) Melting Assay. FRET melting studies with DNA sequences

https://dx.doi.org/10.1021/acsomega.0c03675
ACS Omega 2020, 5, 27332−27343

Table 3. Percentage Growth of Cancer Cells Treated with Compounds 16a−e at a Dose of 10 μM

cell lines	compound code				
	16a	16b	16c	16d	16e
Leukemia					
CCRF-CEM	80.22	88.04	97.38	101.53	101.57
HL-60 (TB)	98.35	99.55	99.05	100.80	99.82
K-562	44.82	54.78	77.07	92.78	75.30
MOLT-4	64.33	74.19	88.12	92.44	92.11
RPMI-8226	62.34	75.07	88.56	98.70	88.16
SR	68.10	80.58	98.05	92.78	97.00
Non-Small Cell Lung Cancer					
A549/ATCC	59.15	72.72	87.91	95.65	92.18
EKVX	70.09	78.49	90.97	95.58	91.78
HOP-62	68.97	77.78	94.29	97.31	94.75
HOP-92	70.15	87.22	83.00	95.10	86.33
NCI-H226	73.55	82.19	87.96	100.50	90.45
NCI-H23	67.72	82.43	86.05	92.43	96.24
NCI-H322M	89.94	94.29	102.92	98.57	102.78
NCI-H460	73.33	86.16	97.71	104.41	99.39
NCI-H522	58.18	67.43	76.39	85.73	82.98
Colon Cancer					
COLO 205	76.58	95.47	104.94	110.37	112.22
HCC-2998	84.49	96.41	88.39	104.18	99.67
HCT-116	39.67	56.75	84.36	94.87	86.28
HCT-15	59.49	70.77	86.89	100.71	95.70
HT29	36.02	49.22	84.27	100.63	87.22
KM12	75.02	86.71	93.93	102.69	100.52
SW-620	72.04	83.60	95.19	105.74	95.41
CNS Cancer					
SF-268	69.46	77.34	89.71	94.39	91.22
SF-295	78.46	87.77	90.64	97.51	93.95
SF-539	90.55	100.79	104.33	100.38	102.47
SNB-19	85.08	89.96	85.98	87.01	89.85
SNB-75	71.88	83.86	76.68	91.74	96.08
U251	82.30	82.13	92.86	91.07	94.12
Melanoma					
LOX IMVI	79.81	88.84	92.97	97.67	97.29
MALME-3M	81.71	87.68	92.72	111.17	99.40
M14	76.03	85.48	98.93	109.01	101.58

cell lines	compound code				
	16a	16b	16c	16d	16e
Melanoma					
MDA-MB-435	78.90	88.88	97.65	103.80	106.47
SK-MEL-2	82.90	93.09	96.90	104.38	99.20
SK-MEL-28	95.61	101.39	104.95	114.70	113.92
SK-MEL-5	94.24	97.21	99.07	98.92	99.04
UACC-257	85.54	97.67	97.50	102.49	103.32
UACC-62	63.88	65.22	66.32	75.93	78.38
Ovarian Cancer					
IGROV1	62.55	67.05	80.82	85.77	79.66
OVCAR-3	79.31	95.23	97.80	107.31	101.14
OVCAR-4	63.65	79.33	83.64	102.88	96.31
OVCAR-5	82.07	88.79	88.56	98.18	98.89
OVCAR-8	83.79	90.09	95.46	100.69	98.81
NCI/ADR-RES	58.94	70.83	76.67	95.63	79.68
SK-OV-3	80.79	98.18	91.41	99.94	93.62
Renal Cancer					
786−0	79.22	87.65	96.01	97.77	97.79
A498	88.93	102.44	99.79	102.85	104.93
ACHN	79.63	89.56	95.55	98.78	100.18
CAKI-1	46.90	54.08	68.21	70.13	63.20
RXF 393	69.66	92.66	80.83	92.48	92.58
SN12C	69.96	81.35	92.08	99.09	94.48
TK-10	92.06	97.01	102.72	105.97	109.46
UO-31	48.28	56.35	70.33	72.62	65.87
Prostate Cancer					
PC-3	43.51	55.82	75.31	79.50	70.70
DU-145	83.54	99.22	99.00	106.99	103.63
Breast Cancer					
MCF7	62.37	75.94	98.76	93.65	98.51
MDA-MB-231/ ATCC	81.72	89.25	93.93	94.75	94.68
HS 578T	89.25	93.87	93.24	95.37	94.21
BT-549	100.02	99.28	105.31	105.13	110.56
T-47D	49.54	64.16	85.76	86.09	81.52
MDA-MB-468	81.40	91.24	95.45	114.03	105.94
mean % growth	**73.10**	**83.11**	**90.79**	**97.49**	**94.51**

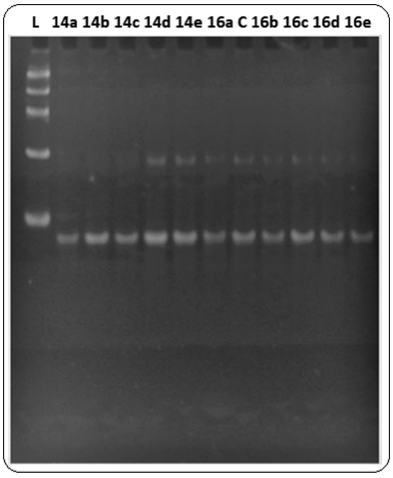

Figure 7. Gel electrophoresis of PCR-stop assay product of the spirooxindole derivatives **14a−e** and **16a−e** in the presence of Pu27 oligonucleotide.

labeled at the 5′ and 3′ ends was performed in an RT-PCR, aiming to evaluate the G4-DNA stabilizing properties of the compounds. The initial screening was made at a concentration of 20 μM of the spirooxindole derivatives **14a−e** and **16a−e**, and the results are presented in Figures 8 and 9. The melting temperature of the DNA G4 has not significantly changed in the presence of the compounds, indicating that these compounds are not G4-DNA ligands.

3. CONCLUSIONS

The methodology employed in the synthesis of spirooxindole derivatives employing α,β-unsaturated carbonyl compounds proved to be highly stereoselective and regioselective. In addition, the one-pot, multicomponent, [3 + 2] cycloaddition reaction described herein is also a catalyst-free reaction with high atom economy and a single-step reaction forming the spirooxindoles efficiently *via in situ* azomethine ylide formation. The result also suggests that ethanol may be utilized as a suitable solvent to construct the spirocyclic framework instead of nonpolar or other polar solvents. This may be attributed to the higher solubilizing capacity and

https://dx.doi.org/10.1021/acsomega.0c03675
ACS Omega 2020, 5, 27332−27343

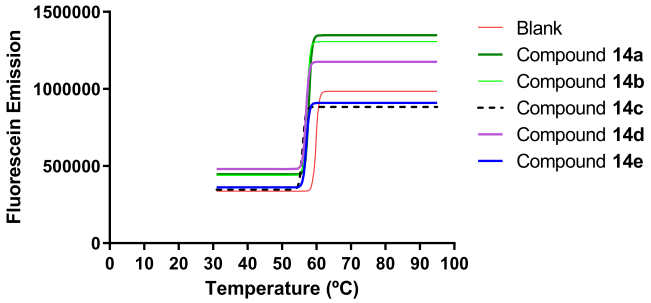

Figure 8. FRET melting assay curve-fitting plots for KRAS21 G4-DNA in the absence (blank) and presence of pyrrolizidine spirooxindole derivatives **14a−e**.

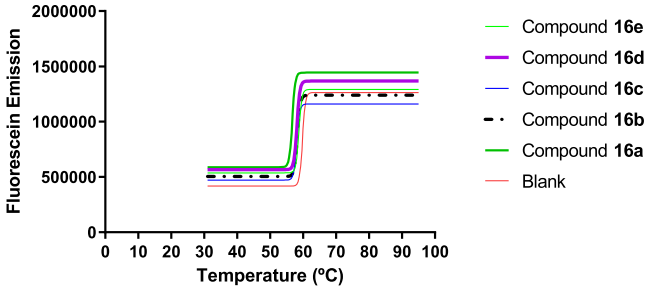

Figure 9. FRET melting assay curve-fitting plots for KRAS21 G4-DNA in the absence (blank) and presence of *N*-methyl spirooxindole derivatives **16a−e**.

optimum boiling temperature of ethanol in comparison to other solvents.

The cytotoxicity assay of the spirooxindole derivatives revealed their selective antiproliferative activity against cancer cell lines. The pyrrolizidine spirooxindole derivative **14b** emerged as a hit molecule emphasizing further hit-to-lead optimization studies to improve the therapeutic efficacy of these molecules. The spirooxindole derivatives could not prove to be G4 interactive ligands. In general, molecules with planar conformations are better G-quadruplex interactive substances. The spiro molecules have an inherent three-dimensional (3D) nature due to rotation at the spiro carbon, and this may be the possible reason that spirocyclic compounds are not suitable ligands for G4 stabilization.

4. EXPERIMENTAL METHODS

4.1. Materials and Equipment. The substituted acetophenones and aldehydes were purchased from HiMedia Laboratories, India. Isatin, proline, sarcosine, and deuterated chloroform ($CDCl_3$) were purchased from Sigma-Aldrich, India. Anhydrous sodium sulfate, precoated TLC plates (silica gel 60 F_{254}), and solvents were purchased from Merck India. All solvents were distilled and dried according to the standard procedures prior to use.

Melting points were determined on a precision digital melting point apparatus (VEEGO Instruments Corporation, India) and are uncorrected. Infrared spectra (wavenumbers in cm^{-1}) were recorded on an ATR-FTIR alpha (Bruker, Germany). The ^1H, ^{13}C, and COSY NMR spectra were obtained on a Bruker Avance-II 400 MHz spectrometer (Bruker Corporation, Billerica) using $CDCl_3$ as a solvent containing tetramethylsilane as the internal standard (chemical shifts in δ, ppm). The spin multiplicities are indicated by the symbols, s (singlet), d (doublet), t (triplet), and m (multiplet). Mass spectra were obtained on a Shimadzu LC-MS 8040 ESI-MS system (Kyoto, Japan). The purity of the spirooxindole derivatives was determined by an high-performance liquid chromatography (RP-HPLC) (Agilent) using a C18 column and acetonitrile/water as solvent. The optical rotation of the compounds was recorded on a digital automatic polarimeter (Lasany, India). The NMR spectra, mass spectra, and HPLC chromatograms of all derivatives as well as 3D structure and SwissADME data of the most active derivative **14b** are given in the Supporting Information.

For the G4 interaction assay, oligonucleotides and fluorophore were purchased from STAB VIDA (Portugal). Taq DNA polymerase and ThermoPol reaction buffer were purchased from New England Biolabs, Portugal, whereas water for dilutions and other chemicals were procured from Sigma, Portugal. RT-PCR plates were purchased from Axygen, Inc., and RT-PCR was performed in a 7300 RT-PCR equipment from Applied Biosystems (AB Sciex Pte. Ltd.). G4 assay experiments were performed in triplicate, and final analysis of the data was carried using nonlinear regression fit with GraphPad Prism v.5.0 software (GraphPad Software, Inc.).

4.2. Synthesis of Substituted α,β-Unsaturated Carbonyl Compounds 11a−e. The substituted acetophenones (**9**) (0.01mol), substituted aldehyde (**10**) (0.01mol), and sodium hydroxide (0.025 mol) were dissolved in methanol (10 mL) and stirred for 5−6 h at room temperature. The reaction mixture was then poured into crushed ice with stirring. The precipitate of the crude product was filtered under vacuum, washed with distilled water, air-dried, and recrystallized with ethanol to yield α,β-unsaturated carbonyl compounds **11a−e**.

*4.2.1. 1,3-Di(p-bromophenyl)prop-2-en-1-one (**11a**).* Light yellow solid (92%); mp 171−173 °C. FTIR (cm^{-1}): 1653, 1588, 1481, 1398, 1324, 1215, 1070, 989, 811, 739, 663. ^1H NMR (400 MHz, $CDCl_3$) δ (ppm): 7.41 (d,1H, *H*C−C═O, *J* = 15 Hz), 7.46 (d, 2H, Ar*H*, *J* = 8 Hz), 7.52 (d, 2H, Ar *H*, *J* = 8 Hz), 7.61 (d, 2H, Ar *H*, *J* = 8 Hz), 7.70 (d,1H, *H*C═C, *J* = 15 Hz), 7.84 (d, 2H, Ar *H*, *J* = 8 Hz); ^{13}C NMR (400 MHz, $CDCl_3$) δ (ppm): 121.96, 125.07, 128.10, 129.84, 130.01, 132, 132.28, 133.62, 136.74, 143.93, 189.06.

*4.2.2. 1-(p-Bromophenyl)-3-(p-chlorophenyl)prop-2-en-1-one (**11b**).* Dark yellow solid (88%); mp 155−157 °C. FTIR (cm^{-1}): 1652, 1586, 1482, 1398, 1323, 1212, 1079, 985, 811, 662. ^1H NMR (400 MHz, $CDCl_3$) δ (ppm): 7.35 (d, 2H, Ar *H*, *J* = 8 Hz), 7.39 (d, 1H, *H*C−C═O, *J* = 15 Hz), 7.53 (d, 2H, Ar *H*, *J* = 8 Hz), 7.60 (d, 2H, Ar *H*, *J* = 8 Hz), 7.71 (d, 1H, *H*C═C, *J* = 15 Hz), 7.84 (d, 2H, Ar *H*, *J* = 8 Hz); ^{13}C NMR (400 MHz, $CDCl_3$) δ (ppm): 121.86, 128.08, 129.31, 129.66, 130.01, 131.99, 133.19, 136.75, 143.85, 189.03.

*4.2.3. 1,3-Di(p-methoxyphenyl)prop-2-en-1-one (**11c**).* Yellow solid (90%); mp 92−94 °C. FTIR (cm^{-1}): 1590, 1505, 1327, 1251, 1164, 1013, 813. ^1H NMR (400 MHz, $CDCl_3$) δ (ppm): 3.85 (s, 3H, −OCH_3), 3.89 (s, 3H, −OCH_3), 6.93 (d, 2H, Ar *H*, *J* = 9 Hz), 6.97 (d, 2H, Ar *H*, *J* = 9 Hz), 7.42 (d, 1H, *H*C−C═O, *J* = 15 Hz), 7.59 (d, 2H, Ar *H*, *J* = 9 Hz), 7.77 (d, 1H, *H*C═C, *J* = 15 Hz), 8.0 (d, 2H, Ar *H*, *J* = 9 Hz); ^{13}C NMR (400 MHz, $CDCl_3$) δ (ppm): 55.40, 55.48, 113.80, 114.15, 114.40, 119.57, 127.83, 130.12, 130.71, 131.37, 143.21, 161.53, 163.29, 188.77.

*4.2.4. 1-(p-Bromophenyl)-3-(3,4,5-trimethoxyphenyl)-prop-2-en-1-one (**11d**).* Pale yellow solid (87%); mp 123−125 °C. FTIR (cm^{-1}) 1664, 1586, 1504, 1452, 1417, 1281, 1124, 989, 815, 769. ^1H NMR (400 MHz, $CDCl_3$) δ (ppm): 4.25 (s, 3H, −OCH_3), 4.27 (s, 6H, 2OCH_3), 7.21 (s, 2H, Ar

https://dx.doi.org/10.1021/acsomega.0c03675
ACS Omega 2020, 5, 27332−27343

H), 7.67 (d, 1H, *HC*−C═O, *J* = 15 Hz), 7.99 (d, 2H, Ar *H*, *J* = 9 Hz), 8.05 (d, 1H, *HC*═C, *J* = 15 Hz), 8.22 (d, 2H, Ar *H*, *J* = 9 Hz); ^{13}CNMR (400 MHz, $CDCl_3$) δ (ppm): 56.27, 61.02, 105.81, 120.87, 127.81, 130.02, 131.93, 137.02, 140.72, 145.61, 153.54, 189.42.

*4.2.5. 1-(p-Bromophenyl)-3-phenyl-prop-2-en-1-one (**11e**).* Pale yellow solid (85%); mp 85−87 °C. FTIR (cm^{-1}) 1654, 1566, 1392, 1326, 1278, 1207, 983, 824, 758, 689. ^{1}H NMR (400 MHz, $CDCl_3$) δ (ppm): 7.40 (t, 3H, Ar *H*, *J* = 3 Hz), 7.43 (d,1H, *HC*−C═O, *J* = 15 Hz), 7.61 (d, 4H, Ar *H*, *J* = 9 Hz), 7.77 (d, 1H, *HC*═C, *J* = 15 Hz), 7.85 (d, 2H, Ar *H*, *J* = 9 Hz); ^{13}C NMR (400 MHz, $CDCl_3$) δ (ppm): 121.51, 127.91, 128.53, 129.02, 130.04, 130.77, 131.95, 134.71, 136.95, 145.43, 189.40.

4.3. Synthesis of Pyrrolizidine Spirooxindole Derivatives 14a−e. A mixture of appropriate α,β-unsaturated carbonyl compounds **11a−e** (0.003 mol), isatin (**12**) (0.004 mol), and L-proline (**13**) (0.004 mol) was refluxed together in absolute ethanol (10 mL) for 5 h. After completion of the reaction, as indicated by TLC (chloroform/*n*-hexane = 4:1), the reaction mixture was filtered hot and the filtrate was concentrated under vacuum to obtain the crude product. The crude was then dried and recrystallized from ether to obtain **14a−e**.

*4.3.1. p-Bromophenyl-{1-(p-bromophenyl)-[3-spiro-(indolin-2-one-3-yl)]-hexahydro-1H-pyrrolizin-2-yl}methanone (**14a**).* White solid (86%), mp 188−191 °C. Purity in % (HPLC): 100%. FTIR (cm^{-1}): 3845, 3743, 1719, 1544, 1463, 1176, 1067, 1001, 744, 646. ESI-MS (*m*/*z*), calcd for $C_{27}H_{22}Br_2N_2O_2$ = 564, found 565 $[M + H]^+$, 567 $[MH + 2]^+$, 569 $[MH + 4]^+$. ^{1}H NMR (400 MHz, $CDCl_3$) δ(ppm): 1.70−2.05 (m, 4H, *Hb* & *Hc*), 2.60−2.71 (m, 2H, *Ha*), 3.87 (t, 1H, *He*, *J* = 12 Hz), 4.19−4.24 (m, 1H, *Hd*), 4.80 (d, 1H, *Hf*, *J* = 11.60 Hz), 6.62−7.46 (m, 12H, Ar *H*), 8.19 (s, 1H, N*H*); ^{13}C NMR (400 MHz, $CDCl_3$) δ (ppm): 27.20, 30.54, 48.13, 52.44, 64.68, 71.77, 73.32, 120.93, 121.49, 122.43, 124.24, 124.86, 127.57, 128.19, 129.38, 129.62, 129.81, 131.50, 131.86, 135.74, 138.69, 140.36, 180.34, 195.96.

*4.3.2. p-Bromophenyl-{1-(p-chloro-phenyl)-[3-spiro-(indolin-2-one-3-yl)]-hexahydro-1H-pyrrolizin-2-yl}methanone (**14b**).* White solid (80%); mp 195−197 °C. Purity in % (HPLC): 100%. $[\alpha]^{25}$ = +17°. FTIR (cm^{-1}): 3852, 3740, 1711, 1525, 1468, 1181, 997, 745. ESI-MS (*m*/*z*), calcd for $C_{27}H_{22}BrClN_2O_2$ = 520, found 521 $[M + H]^+$, 523 $[MH + 2]^+$, 525 $[MH + 4]^+$. ^{1}H NMR (400 MHz, $CDCl_3$) δ (ppm): 1.75−2.06 (m, 4H, *Hb* & *Hc*), 2.60−2.73 (m, 2H, *Ha*), 3.88 (t, 1H, *He*, *J* = 12 Hz), 4.19−4.25 (m, 1H, *Hd*), 4.80 (d, 1H, *Hf*, *J* = 11.20 Hz), 6.61−7.46 (m, 12H, Ar *H*), 8.07 (s, 1H, N*H*); ^{13}C NMR (400 MHz, $CDCl_3$) δ (ppm): 27.26, 30.63, 48.27, 52.36, 64.52, 71.89, 73.62, 110.38, 122.45, 124.78, 127.44, 128.30, 128.8, 128.91, 129.38, 129.44, 129.67, 131.48, 132.83, 135.58, 138.09, 140.57, 180.98, 195.95.

*4.3.3. p-Methoxyphenyl-{1-(p-methoxyphenyl)-[3-spiro-(indolin-2-one-3-yl)]hexahydro-1H-pyrrolizin-2-yl}-methanone (**14c**).* White solid (87%); mp 239−241 °C. Purity in % (HPLC): 97.32%. FTIR (cm^{-1}): 3852, 3740, 1701, 1524, 1176, 745. ESI-MS (*m*/*z*), calcd for $C_{29}H_{28}N_2O_4$ = 468, found 469 $[M + H]^+$. ^{1}H NMR (400 MHz, $CDCl_3$) δ (ppm): 1.50−2.08 (m, 4H, *Hb* & *Hc*), 2.64−2.76 (m, 2H, Ha), 3.71 (d, 6H, $-OCH_3$), 3.90 (t, 1H, *He*, *J* = 11 Hz), 4.25−4.29 (m, 1H, *Hd*), 4.85 (d, 1H, *Hf*, *J* = 11.60 Hz), 6.57−7.54 (m, 12H, Ar *H* & 1H, N*H*); ^{13}C NMR (400 MHz, $CDCl_3$) δ (ppm): 27.35, 30.77, 48.28, 52.32, 55.22, 55.28, 63.95, 71.97, 73.91, 110.01, 113.31, 114.06, 122.23, 125.25, 127.69, 129.03, 129.27, 130.14, 130.27, 130.81, 131.79, 140.43, 158.49, 163.30, 181.10, 195.11.

*4.3.4. p-Bromophenyl-{1-(3,4,5-trimethoxyphenyl)-[3-spiro-(indolin-2-one-3-yl)]hexahydro-1H-pyrrolizin-2-yl}-methanone (**14d**).* White solid (76%); mp 205−207 °C. Purity in % (HPLC): 99.48%. FTIR (cm^{-1}): 3871, 3789, 3723, 3633, 2829, 1684, 1586, 1510, 1459, 1327, 1121, 997, 832, 754, 642. ESI-MS (*m*/*z*), calcd for $C_{30}H_{29}BrN_2O_5$ = 576, found 577 $[M + H]^+$, 579 $[MH + 2]^+$. ^{1}H NMR (400 MHz, $CDCl_3$) δ (ppm): 1.76−2.07 (m, 4H, *Hb* & *Hc*), 2.65−2.66 (m, 2H, *Ha*), 3.80−3.89 (m, 10H, $-(OCH_3)_3$ & *He*), 4.26 (m, 1H, *Hd*), 4.82 (d, 1H, *Hf*, *J* = 11.20 Hz), 6.61−7.37 (m, 10H, Ar *H*), 7.86 (s, 1H, N*H*); ^{13}C NMR (400 MHz, $CDCl_3$) δ (ppm): 27.39, 30.98, 48.14, 53.23, 56.21, 60.75, 64.65, 71.87, 73.74, 104.99, 110.12, 122.42, 124.88, 127.56, 128.20, 129.43, 129.60, 131.50, 135.30, 135.78, 136.96, 140.38, 153.31, 180.45, 196.13.

*4.3.5. p-Bromophenyl-{(1-phenyl)-[3-spiro-(indolin-2-one-3-yl)]hexahydro-1H-pyrrolizin-2-yl} methanone (**14e**).* White solid (79%); mp 163−165 °C. Purity in % (HPLC): 100%. FTIR (cm^{-1}): 3849, 3785, 3699, 3638, 3202, 2847, 1679, 1586, 1465, 1392, 1334, 1188, 1071, 985, 797, 746, 693. ESI-MS (*m*/*z*), calcd for $C_{27}H_{23}BrN_2O_2$ = 486, found 487 $[M + H]^+$, 489 $[MH + 2]^+$. ^{1}H NMR (400 MHz, $CDCl_3$) δ (ppm): 1.76−2.06 (m, 4H, *Hb* & *Hc*), 2.60−2.75 (m, 2H, *Ha*), 3.89 (t, 1H, *He*, *J* = 11 Hz), 4.20−4.25 (m, 1H, *Hd*), 4.86 (d, 1H, *Hf*, *J* = 11.40 Hz), 6.57−7.46 (m, 13H, Ar *H*), 8.15 (s, 1H, N*H*); ^{13}C NMR (400 MHz, $CDCl_3$) δ (ppm): 27.17, 30.60, 48.24, 52.85, 64.19, 72,73.64, 110.33, 122.29, 124.75, 127, 127.41, 127.98, 128.09, 128.65, 129.32, 129.52, 129.59, 131.34, 131.84, 135.58, 139.40, 140.54, 180.98, 195.94.

4.4. Synthesis of *N*-Methyl Spirooxindole Derivatives 16a−e. A mixture of appropriate α,β-unsaturated carbonyl compounds **11a−e** (0.003 mol), isatin (**12**) (0.004 mol), and sarcosine (**15**) (0.004 mol) was refluxed in ethanol (10 mL) for 5 h. After completion of the reaction, as indicated by TLC (chloroform/*n*-hexane = 4:1), the reaction mixture was filtered hot and the filtrate was concentrated under vacuum to obtain the crude product. The crude was then dried and recrystallized from ether to obtain **16a−e**.

*4.4.1. p-Bromophenyl-{4-(p-bromophenyl)-[2-spiro-(indolin-2-one-3-yl)]N-methyl-pyrrolidin-3-yl}methanone (**16a**).* White solid (93%); mp 221−223 °C. Purity in % (HPLC): 97.12%. $[\alpha]^{25}$ = +14°. FTIR (cm^{-1}): 3897, 3732, 3549, 1722, 1674, 1580, 1469, 1391, 1327, 1181, 1067, 1005, 825, 739. ESI-MS (m/z), calcd for $C_{25}H_{20}Br_2N_2O_2$ = 538, found 541 $[MH + 2]^+$, 536 $[M - 2H]^-$, 538 $[(M - 2H) + 2]^-$, 540 $[(M - 2H) + 4]^-$. ^{1}H NMR (400 MHz, $CDCl_3$) δ (ppm): 2.22 (s, 3H, N-CH_3), 3.44−3.51 (m, 1H, *Hb*), 3.62 (t, 1H, *Hb*, *J* = 9 Hz), 4.39 (d, 1H, *Hd*, *J* = 9.28 Hz), 4.45−4.52 (m, 1H, *Hc*), 6.51−7.46 (m, 12H, Ar *H*), 7.61 (s, 1H, N*H*); ^{13}C NMR (400 MHz, $CDCl_3$) δ (ppm): 34.91, 43.91, 60.19, 62.93, 73.47, 109.47, 120.80, 123.11, 126.65, 126.77, 128, 129.13, 129.39, 129.91, 131.41, 131.79, 135.83, 140.37, 140.43, 179.87, 196.28

*4.4.2. p-Bromophenyl-{4-(p-chlorophenyl)-[2-spiro-(indolin-2-one-3-yl)]N-methyl-pyrrolidin-3-yl}methanone (**16b**).* White solid (81%); mp 230−232 °C. Purity in % (HPLC): 100%. FTIR (cm^{-1}): 3904, 3866, 3729, 3610, 2922, 2855, 1722, 1674, 1583, 1466, 1392, 1324, 1177, 1072, 1004, 935, 825, 777, 739, 676. ESI-MS (*m*/*z*), calcd for $C_{25}H_{20}BrClN_2O_2$ = 494, found 492 $[M - 2H]^-$, 494 $[(M - 2H) + 2]^-$, 496 $[(M - 2H) + 4]^-$. ^{1}H NMR (400 MHz, $CDCl_3$) δ (ppm): 2.23 (s,

https://dx.doi.org/10.1021/acsomega.0c03675
ACS Omega 2020, 5, 27332−27343

3H, N−CH_3), 3.44−3.49 (m, 1H, *Hb*), 3.63 (t, 1H, *Hb*, *J* = 9 Hz), 4.41 (d, 1H, *Hd*, *J* = 9.24 Hz), 6.54−7.49 (m, 12H, Ar *H*), 8.05 (s, 1H, N*H*); ^{13}C NMR(400 MHz, $CDCl_3$) δ (ppm): 34.90, 43.85, 60.24, 62.98, 73.41, 109.38, 123.10, 126.68, 126.77, 127.97, 128.81, 129.11, 129.31, 129.36, 129.51, 130.01, 131.40, 132, 132.70, 135.84, 139.85, 140.31, 143.92, 179.74, 196.28.

*4.4.3. p-Methoxyphenyl-{4-(p-methoxyphenyl)-[2-spiro-(indolin-2-one-3-yl)]N-methyl-pyrrolidin-3-yl}methanone-(**16c**).* White solid (83%); mp 152−154 °C. Purity in % (HPLC): 100%. FTIR (cm^{-1}): 3851, 3740, 2925, 1657, 1508, 1461, 1246, 1167, 1020, 829, 742. ESI-MS (*m*/*z*), calcd for $C_{27}H_{26}N_2O_4$ = 442, found 443 $[M + H]^+$; ^{1}H NMR (400 MHz, $CDCl_3$) δ (ppm): 2.23 (s, 3H, −NCH_3), 3.43−3.47 (m, 1H, *Hb*), 3.63 (t, 1H, *Hb*, *J* = 9 Hz), 3.71 (s, 3H, −OCH_3), 3.77 (s, 3H, OCH_3), 4.49−4.53 (m, 2H, *Hb* & *Hc*), 6.53−7.47 (m, 12H, Ar *H*), 7.99 (s, 1H, N*H*); ^{13}C NMR (400 MHz, $CDCl_3$) δ (ppm): 35.01, 43.96, 55.25, 55.29, 60.53, 62.53, 73.58, 122.91, 127, 127.30, 128.92, 129.13, 130, 130.51, 133.53, 140.14, 158.44, 163.12, 179.64, 195.69.

*4.4.4. p-Bromophenyl-{4-(3,4,5-trimethoxyphenyl)-[2-spiro-(indolin-2-one-3-yl)]N-methyl-pyrrolidin-3-yl}-methanone (**16d**).* White solid (75%); mp 176−178 °C. Purity in % (HPLC): 98.58%. FTIR (cm^{-1}): 3863, 1720, 1674, 1585, 1460, 1326, 1240, 1181, 1121, 1003, 830, 746. ESI-MS (*m*/*z*), calcd for $C_{28}H_{27}BrN_2O_5$ = 550, found 549 $[M - H]^-$, 551 $[(M - H) + 2]^-$. ^{1}H NMR (400 MHz, $CDCl_3$) δ (ppm): 2.23 (s, 3H, N−CH_3), 3.45−3.49 (m, 1H, *Hb*), 3.65−3.69 (m, 1H, *Hb*), 3.82 (s, 3H, OCH_3), 3.90 (s, 6H, −OCH_3), 4.45−4.48 (m, 2H, *Hb* & *Hc*), 6.52−7.32 (m, 10H, Ar *H*), 7.74 (s, 1H, N*H*); ^{13}C NMR (400 MHz, $CDCl_3$) δ (ppm): 34.95, 44.83, 56.19, 60.34, 60.77, 62.96, 73.48, 105.13, 109.35, 123.01, 126.71, 126.77, 127.91, 129.18, 129.31, 131.39, 135.95, 136.87, 137.25, 140.35, 153.29, 179.73, 196.62.

*4.4.5. p-Bromophenyl-{4-(phenyl)-[2-spiro-(indolin-2-one-3-yl)]N-methyl-pyrrolidin-3-yl}-methanone (**16e**).* White solid (78%); mp 193−195 °C. Purity in % (HPLC): 100%. IR (cm^{-1}): 3943, 3864, 3776, 3571, 3173, 3057, 2795, 2040, 1721, 1672, 1585, 1467, 1392, 1327, 1172, 1072, 1005, 938, 829, 747, 698. ESI-MS (*m*/*z*), calcd for $C_{25}H_{21}BrN_2O_2$ = 460, found 459 $[M - H]^-$, 461 $[(M - H) + 2]^-$. ^{1}H NMR (400 MHz, $CDCl_3$) δ (ppm): 2.23 (s, 3H, −NCH_3), 3.46−3.51 (m, 1H, *Hb*), 3.68 (t, 1H, *Hb*, *J* = 9 Hz), 4.49−4.57 (m, 2H, *Hb* & *Hc*), 6.92−7.55 (m, 13H, Ar *H*), 8.25 (s, 1H, N*H*); ^{13}C NMR (400 MHz, $CDCl_3$) δ (ppm): 34.96, 44.51, 60.46, 62.89, 73.58, 109.44, 123.05, 126.84, 126.88, 126.93, 127.39, 127.85, 128.13, 128.37, 128.70, 128.74, 129.18, 129.29, 129.68, 131.36, 131.94, 135.57, 136, 140.45, 141.34, 143.37, 180.04, 196.49.

4.5. Antineoplastic Activity. *4.5.1. In Vitro Cancer Cell Line Assay.* The cytotoxicity assay was performed as per the protocol of NCI on 60 different cancer cell lines of nine tissue origins using a sulforhodamine B (SRB) assay.[20]

4.5.2. G-Quadruplex (G4) Interaction Assay. The G-quadruplex interaction assay was performed using methodologies previously reported by the authors.[21,22]

4.5.2.1. FRET Melting Assay. The capacity of compounds to interact and stabilize/destabilize DNA G4 or duplex structures was assessed using a FRET melting assay. Tagged G4-forming oligonucleotides (Table 4) at 0.4 μM were annealed by heating at 90−95 °C for 10 min, followed by slow cooling to room temperature. Stock solutions of compounds (1 mM) were prepared in 10% DMSO. Subsequent dilutions were performed using FRET buffer. Annealed DNA (50 μL) and test compound solutions (50 μL) were distributed across 96-well RT-PCR plates (PCR-96-FLT-C, Axygen, Inc). Fluorescence readings (performed in a 7300 RT-PCR equipment from Applied Biosystems) were taken at intervals of 0.5 °C in the range 31−95 °C, with the temperature being maintained for 30 s prior to each reading. Experiments were performed in triplicate. Final analysis of the data was carried out with GraphPad Prism v.5.0 (GraphPad Software, Inc., La Jolla, CA). The advanced curve-fitting function in GraphPad Prism (nonlinear regression fit) was used for the calculation of ΔT_m values. Only results with fitting r^2 values >0.75 (std error < 0.25) were considered.

Table 4. Synthetic Oligonucleotides Used in FRET Experiments

code	sequence	ΔT_m (°C)	topology
KRAS21R	5′-FAM-AGG GCG GTG TGG GAA GAG GGA-TAMRA-3′	52	parallel G4
Telo21	5′-FAM-GGG TTA GGG TAG GGT TAG GGG-TAMRA-3′	57	hybrid G4
T-Loop	5′-FAM-TAT AGC TAT ATT TTT TTA TAG CTA TA-TAMRA-3′	53	duplex

4.5.2.2. Polymerase-Stop Assay. Synthetic oligonucleotides enclosing the quadruplex-forming sequences Pu27, the corresponding complementary reverse sequence, and, as negative control, the mutated sequences unable to fold into a G4 structure (Pu27mut) were used for the experiment. PCR products from reaction mixtures containing each quadruplex-forming oligonucleotide (or the mutated), the complementary oligonucleotide, deoxynucleotides (DNTPs), Taq polymerase, and different concentrations of compounds were analyzed on 15% nondenaturing polyacrylamide gels. The DNA sequences used in this assay are presented in Table 5.

Table 5. DNA Sequences Used in Polymerase-Stop Assay

primer code	sequence
Pu27	5′ TGGGGAGGGTGGGGAGGGTGGGGAAGG 3′
Pu27mut	5′ TGGGGAGGGTGGAAAGGGTGGGGAAGG 3′
Rev	5′ ATCGAATCGCTTCTCGTCCTTCCCCA 3′

■ ASSOCIATED CONTENT

Supporting Information

The Supporting Information is available free of charge at https://pubs.acs.org/doi/10.1021/acsomega.0c03675.

^{1}H, ^{13}C and COSY NMR spectra, mass spectra, and HPLC chromatograms of the synthesized compounds (Figures S1−S52) as well as 3D structure and SwissADME data of the most active derivative **14b** (PDF)

■ AUTHOR INFORMATION

Corresponding Author

Pratap Chandra Acharya − *Department of Pharmacy, Tripura University, Suryamaninagar, Agartala 799022, India;* orcid.org/0000-0002-5432-8787; Phone: +91 381 237 9406; Email: pratapacharya@tripurauniv.in; Fax: +91 381 237 4802

https://dx.doi.org/10.1021/acsomega.0c03675
ACS Omega 2020, 5, 27332−27343

Authors

Rajat Ghosh − *Department of Pharmacy, Tripura University, Suryamaninagar, Agartala 799022, India*

Jorge B. Vitor − *Faculty of Pharmacy, University of Lisbon, Lisbon 1649-003, Portugal;* orcid.org/0000-0001-6486-3444

Eduarda Mendes − *Faculty of Pharmacy, University of Lisbon, Lisbon 1649-003, Portugal*

Alexandra Paulo − *Faculty of Pharmacy, University of Lisbon, Lisbon 1649-003, Portugal;* orcid.org/0000-0003-1433-5402

Complete contact information is available at: https://pubs.acs.org/10.1021/acsomega.0c03675

Author Contributions

The study was led and supervised by P.C.A. with the research idea, conception, design of synthesis schemes, analysis, interpretation of data, and writing and review of the manuscript. R.G. performed the synthesis experiments, characterization, interpretation of the analytical data, and wrote the manuscript. A.P. supervised the G4 assay, and analyzed and interpreted the data. P.C.A., J.B.V., and E.M. performed the G4 assay of the synthesized compounds and analyzed the data.

Notes

The authors declare no competing financial interest.

■ ACKNOWLEDGMENTS

This research work was supported by grants from the Council of Scientific & Industrial Research (CSIR), New Delhi [CSIR Extramural Research Grant No. 02(0329)/17/EMR], and the European Molecular Biology Organization (EMBO), Heidelberg [EMBO STF No. 7702], sanctioned to the principal investigator P.C.A. A.P. acknowledges FCT (Portugal) for financial support through project grant PTDC/QUI-QOR/29664/2017 and FCT and COMPETE Program (SAICT-PAC/0019/2015). J.B.V. research was financed by New England Biolabs, Inc. The authors express their gratitude to National Cancer Institute (NCI), Bethesda, for carrying out the *in vitro* cytotoxicity assay, Dr. Rakesh Yadav, Department of Pharmacy, Banasthali Vidyapith, Rajasthan, for providing the NMR spectra, and Dr. Nitesh Sahu for the HPLC and ESI-MS data.

■ REFERENCES

(1) Acharya, P. C.; Bansal, R.; Kharkar, P. S. Hybrids of steroid and nitrogen mustard as antiproliferative agents: Synthesis, in vitro evaluation and in silico inverse screening. *Drug Res.* **2018**, *68*, 100−103.

(2) Senwar, K. R.; Sharma, K. P.; Reddy, T. S.; Jeengar, M. N.; Nayak, V. L.; Naidu, V. G. M.; Kamal, A.; Shankaraiaha, N. Spirooxindole-derived morpholine-fused-1,2,3-triazoles: Design, synthesis, cytotoxicity and apoptosis inducing studies. *Eur. J. Med. Chem.* **2015**, *102*, 413−424.

(3) Zhang, M.; Yang, W.; Qian, M.; Zhao, T.; Yang, L.; Zhu, C. Iodine-promoted three-component reaction for the synthesis of spirooxindoles. *Tetrahedron* **2018**, *74*, 955−961.

(4) Lotfy, G.; Ashry, E. S. H. E.; Said, M. M.; Tamany, E. S. E.; Aziz, Y. M. A.; Al-Dhfyan, A.; Al-Majid, A. M.; Barakat, A. Regio- and stereoselective synthesis of new spirooxindoles via 1,3-dipolar cycloaddition reaction: Anticancer and molecular docking studies. *J. Photochem. Photobiol., B* **2018**, *180*, 98−108.

(5) Tiwari, S.; Pathak, P.; Sagar, R. Efficient synthesis of new 2,3-dihydrooxazole-spirooxindoles hybrids as antimicrobial agents. *Bioorg. Med. Chem. Lett.* **2016**, *26*, 2513−2516.

(6) Yu, B.; Yu, D. Q.; Liu, H. M. Spirooxindoles: promising scaffolds for anticancer agents. *Eur. J. Med. Chem.* **2015**, *97*, 673−698.

(7) Galvis, C. E. P.; Kouznetsov, V. V. Regio- and stereoselective synthesis of spirooxindole 1′-nitro pyrrolizidines with five concurrent stereocenters under aqueous medium and their bioprospection using the zebrafish (*Danio rerio*) embryo model. *Org. Biomol. Chem.* **2013**, *11*, 7372−7386.

(8) Zhou, R.; Wu, Q.; Guo, M.; Huang, W.; He, X.; Yang, L.; Peng, F.; He, G.; Han, B. Organocatalytic cascade reaction for the asymmetric synthesis of novel chroman-fused spirooxindoles that potently inhibit cancer cell proliferation. *Chem. Commun.* **2015**, *51*, 13113−13116.

(9) Yu, B.; Yu, Z.; Qi, P.; Yu, D.; Liu, H. Discovery of orally active anticancer candidate CFI-400945 derived from biologically promising spirooxindoles: success and challenges. *Eur. J. Med. Chem.* **2015**, *95*, 35−40.

(10) Yang, J.; Hu, Y.; Li, Q.; Yu, F.; Cao, J.; Fang, D.; Huang, Z.; Shi, D. Efficient and regioselective synthesis of novel functionalized dispiropyrrolidines and their cytotoxic activities. *ACS Comb. Sci.* **2014**, *16*, 139−145.

(11) Kidwai, M.; Jain, A.; Nemaysh, V.; Kumar, R.; Luthra, P. M. Efficient entry to diversely functionalized spirooxindoles from isatin and their biological activity. *Med. Chem. Res.* **2013**, *22*, 2717−2723.

(12) Zhao, Y.; Liu, L.; Sun, W.; Lu, J.; McEachern, D.; Xiaoqin, L.; Yu, S.; Bernard, D.; Ochsenbein, P.; Ferey, V.; Carry, J. C.; Deschamps, J. R.; Sun, D.; Wang, S. Diastereomeric spirooxindoles as highly potent and efficacious MDM2 inhibitors. *J. Am. Chem. Soc.* **2013**, *135*, 7223−7234.

(13) Rajakumar, P.; Thirunarayanan, A.; Raja, S. Synthesis and antibacterial activity of novel *N*-methyl pyrrolidine dendrimers via [3+2] cycloaddition. *Proc. Natl. Acad. Sci., India, Sect. A* **2014**, *84*, 371−379.

(14) Winter, E.; Locatelli, C.; Dipietro, A.; Creczynski-Pasa, T. B. Recent trends of chalcones potentialities as antiproliferative and antiresistance agents. *Anti-Cancer Agents Med. Chem.* **2015**, *15*, 592−604.

(15) Duarte, A. R.; Cadoni, E.; Ressurreicao, A. S.; Moreira, R.; Paulo, A. Design of modular G-quadruplex ligands. *ChemMedChem.* **2018**, *13*, 869−893.

(16) Neidle, S. Quadruplex nucleic acids as targets for anticancer therapeutics. *Nat. Rev. Chem.* **2017**, *1*, No. 0041.

(17) Bansal, R.; Acharya, P. C. Synthesis and antileukemic activity of 16*E*-[4-(2-carboxy)ethoxybenzylidene]-androstene amides. *Steroids* **2012**, *77*, 552−557.

(18) Acharya, P. C.; Bansal, R. Synthesis and antiproliferative activity of hydroximino androstene derivatives. *Arch. Pharm. Chem. Life Sci.* **2014**, *347*, 193−199.

(19) Gorli, V. N.; Srinivasan, R. Synthesis of spirooxindole analogues from 2-cyclopropyl-4-(4-fluorophenyl)quinoline-3-carbaldehyde. *Synth. Commun.* **2020**, *50*, 516−525.

(20) https://dtp.cancer.gov/discovery_development/nci-60/methodology.htm (accessed on July 26, 2020).

(21) Lavrado, J.; Brito, H.; Borralho, P. M.; Ohnmacht, S. A.; Kim, N. S.; Leitão, C.; Pisco, S.; Gunaratnam, M.; Rodrigues, C. M.; Moreira, R.; Neidle, S.; Paulo, A. KRAS oncogene repression in colon cancer cell lines by G-quadruplex binding indolo [3, 2-c] quinolines. *Sci. Rep.* **2015**, *5*, No. 9696.

(22) Mendes, E.; Cadoni, E.; Carneiro, F.; Afonso, M. B.; Brito, H.; Lavrado, J.; dos Santos, D. J.; Vítor, J. B.; Neidle, S.; Rodrigues, C. M.; Paulo, A. Combining 1,3-ditriazolylbenzene and quinoline to discover a new G-quadruplex-interactive small molecule active against cancer stem-like cells. *ChemMedChem.* **2019**, *14*, 1325−1328.